Petroleum and Coal

Article **Open Access**

Evaluation of Local Hydrate Inhibitors in a Gas Dominated Flow Loop

Nakwaasah Otua Ledum[1], Uche Osokogwu[1] and Okon Efiong Okon[2]*

[1] *Department of Petroleum and Gas Engineering, University of Port Harcourt, Choba, Rivers State, Nigeria*
[2] *World Bank Africa Centre of Excellence in Oilfield Chemicals Research (ACE-CEFOR), University of Port Harcourt, Choba, Rivers State, Nigeria*

Received April 28, 2025; Accepted August 27, 2025

Abstract

This work evaluates the performance of four natural hydrate inhibitors: Asteraceae Extract (AE), Meliaceae Extract (ME), Annonaceae Extract (ANE), and Penaeus monodon Extract (PE) and a kinetic hydrate inhibitor, 2-(Dimethylamino)ethylmethacrylate (DIMETH), using a laboratory flow loop to simulate the offshore pipeline conditions. The performance of each inhibitor was evaluated by monitoring pressure and temperature variations with time, final and initial pressure versus time, and inhibitor efficiency—all fundamental parameters affecting hydrate nucleation and growth. For AE, the pressure drops from 150 psi to 120 psi, 126 psi, and 125 psi at 0.01 wt.%, 0.02 wt.%, and 0.03 wt.%, respectively. ME showed pressure drops of 115 psi, 109 psi, and 129 psi at corresponding concentrations. ANE showed drastic pressure changes of 108 psi, 123 psi, and 119 psi and similar temperature stabilization. PE showed moderate performance with 116 psi, 124 psi, and 118 psi of pressure drops at corresponding concentrations. The conventional inhibitor showed a consistent performance with 115 psi, 118 psi, and 120 psi pressure change at 0.01 wt.%, 0.02 wt.% and 0.03 wt.%, respectively. The plots for the pressure, temperature, and time showed that AE performed better than the rest of the inhibitors at all weight percentages. Though others showed promising results too, the fact that AE is eco-friendly and biodegradable makes it the strongest candidate for field trials.

Keywords: *Kinetic hydrate inhibitor; Low dosage hydrate inhibitors; Plant extracts; Hydrate flow loop; Inhibition efficiency.*

1. Introduction

Gas hydrates are crystalline compounds in which gas molecules, such as methane, become trapped within water molecules under conditions of low temperature and high pressure. Naturally, hydrates are found in marine sediments and permafrost regions, representing significant sources of energy but also posing substantial difficulties during oil and gas operations [1-2]. Their energy potential lies in storing enormous quantities of gas in a compact form; they therefore represent a potentially vast source of unconventional energy [2]. Kvenvolden [3] mentioned "an estimate of global reserves of methane hydrates which is more than twice as great as coal, oil, and conventional natural gas combined, suggesting that they represent future energy." However, hydrate formation poses serious hazards in the oil and gas industry during production, transportation, and storage. The deposition of hydrates in pipelines and equipment causes operational disruptions and safety concerns, as well as potentially high remediation costs [4-5].

Indeed, many offshore deep-water drilling and production operations have faced hydrate-related flow assurance problems because the thermodynamic conditions during these tasks are quite suitable for hydrate formation [6]. Over the years, various methods have been developed to manage hydrate risks, mainly using thermodynamic inhibitors such as methanol (MeOH) and monoethylene glycol (MEG), which lower the freezing point of water and thus hinder hydrate nucleation [7]. Although effective, these conventional inhibitors require high

dosages, pose environmental hazards, and incur significant operational costs. This highlights the need for greener, environmentally friendly, and more cost-effective alternatives [8].

A new type of low-dosage hydrate inhibitors (LDHIs) has emerged as an alternative to thermodynamic inhibitors. LDHIs can be generally divided into two main groups: kinetic hydrate inhibitors (KHIs) and anti-agglomerants (AAs). KHIs slow down hydrate nucleation and growth, while AAs stop hydrate particles from clumping together, enabling safer transportation of the hydrate-laden fluid [9-10]. These inhibitors are effective at much lower dosages, resulting in less environmental impact and reduced operational costs [11].

In recent years, focus has shifted towards sustainable alternatives such as bio-based inhibitors that are low in toxicity, highly effective, and biodegradable [12-21]. Inhibitors derived from plants are promising for managing gas hydrate formation because they contain numerous bioactive compounds with hydrate-inhibiting properties. For instance, Elechi *et al.* [19] found that a locally sourced material, LSM, outperformed synthetic inhibitors like DMAEM (2-DIMETH). Similarly, Okon *et al.* [13] demonstrated that locally sourced kinetic hydrate inhibitors (LDKHIs) exhibit better inhibition efficiency and thermal stability than conventional KHIs. The hybrid hydrate inhibitor (HHI) developed by Mbooh *et al.* [22], tested alongside monoethylene glycol (MEG) and N-vinylcaprolactam (N-VCap), showed superior performance at 5, 6, and 7 weight percentages compared to MEG and N-VCap alone. Madueke *et al.* [23] examined the performance of choline chloride-based deep eutectic solvent (DES), MEG, and their combination (DES+MEG) in a flow loop, observing a performance ranking of DES, then MEG, and finally DES+MEG. The optimal result was achieved with 5 wt.% DES+MEG, offering an inhibitory efficiency of 80%, while a lower concentration of 3 wt.% yielded 73.75%. Additionally, Kakwaya *et al.* [24] confirmed the effectiveness of bio-based inhibitors by revealing that hemicellulose extracted from plant gum exudates could efficiently inhibit hydrate formation. This occurs by interfering with the hydrogen bonding network of water molecules, facilitating the formation of hydrate cages.

Among the promising plant-based inhibitors, Meliaceae extracts contain flavonoids, saponins, and alkaloids responsible for antioxidant and hydrate inhibition activities, making them valuable as natural alternatives in gas hydrate management [9]. Similarly, extracts from the Annonaceae family originate from flowering evergreen trees. The bioactive compounds of Annonaceae members are mainly extracted from the fruits, seeds, and leaves. Alkaloids containing quaternary ammonium groups strongly interact with water molecules, inhibiting hydrate formation by adsorbing onto hydrate surfaces [25-26]. Extracts from the Asteraceae family contain a diverse mixture of phytochemicals, including flavonoids, tannins, and saponins, all exhibiting surface activity and hydrate inhibition potential [27-28]. Flavonoids have potent antioxidant properties, and tannins, being high-molecular-weight polyphenolics, interfere with hydrate nucleation and growth [29-31]. Saponins are used as foaming agents that stabilise emulsions by preventing hydrate agglomeration through bubble formation [32-33].

Apart from plant-based inhibitors, chitosan, a biodegradable biopolymer extracted from crustacean shells, has also been researched for hydrate inhibition. Chitosan is of high molecular weight and possesses structural features capable of forming strong hydrogen bonds with water molecules, creating a protective barrier on the hydrate surface, which effectively inhibits hydrate growth [34]. Being environmentally friendly and effective at low concentrations, chitosan offers a promising alternative to synthetic inhibitors.

2. Materials and methods

The materials used in this study included ice blocks and compressed natural gas (CNG) weighing 16.46 g, with a specific gravity of 0.5, composed of 98.44% methane and 1.56% carbon dioxide. The CNG was procured from Total Support Gas Company in Port Harcourt, Nigeria. Inhibitors used were water soluble and they are: *Asteraceae family extract,* Meliaceae family extract, Anonnaceae family extract, Penaeus monodon shell extract and 2-(Dimethylamino)ethylmethacrylate.

The leaves of these inhibitors were collected from a farm in Etche Community in Port Harcourt, while the shell extract was obtained from Rumuokoro market. The plant extractions

were conducted at Suano Laboratory Center, and the hydrate experiment was performed at the Petroleum Production Engineering Laboratory, University of Port Harcourt, Nigeria. The natural plant leaves were air-dried at room temperature for several days and then ground into a coarse powder using a blender to increase their surface area for the extraction process. The Soxhlet extraction technique was used, with ethanol as the solvent. Afterwards, the extracts were analyzed via gas chromatography-mass spectrometry (GC-MS). Detailed information about the identified compounds, including their molecular formulae and weights is provided in Tables 1 to 7 while their chemical structures are displayed as Figures 1 to 4.

Table 1. GC–MS analysis of bioactive compounds in ethanol leaf extract of *Vernonia amygalina* of the Asteraceae family.

Name of the compound	Molecular formulae	Molecular weight
Pentadecanoic acid, 14-methylmethylester	$C_{17}H_{34}O_2$	270.45
9,12-Octadecadienoic acid, methyl ester	$C_{19}H_{34}O_2$	294.47
Gypsogenin	$C_{30}H_{46}O_3$	454.69
Vernonioside	$C_{35}H_{56}O_{13}$	684.82
Quercetin	$C_{15}H_{10}O_7$	302.24
9,17-Octadecadienal	$C_{18}H_{32}O$	264.45
Luteolin	$C_{15}H_{10}O_6$	286.24
1,19-Eicosadiene	$C_{20}H_{38}$	278.50
2-Methyl-Z, Z-3,13-octadecadienol	$C_{19}H_{36}O$	280.49

Table 2. Qualitative phytochemicals screening of ethanolic leaf extract of *Vernonia amygdalina* family extract.

Bioactive component	% present in *Vernonia amygdalina*
Tannins	++
Flavonoids	++
Saponins	+++
Alkaloids	++
Sesquiterpene lactone	++

Table 3. GC–MS analysis bioactive compounds in ethanol leaf extract of Meliceae family.

Name of the compound	Molecular formula	Molecular weight
n-Tetracosanol-1	$C_{24}H_{50}O$	354.65
1-Octadecyne	$C_{18}H_{34}$	250.46
9,9-Dimethoxybicyclo [3.3.1] nona-2,4-dione	$C_{11}H_{16}O_4$	212.24
Oleic Acid	$C_{18}H_{34}O_2$	282.46
Octadecane, 1-(ethenyloxy)	$C_{20}H_{40}O_2$	296.53
3-Tetradecyn-1-ol	$C_{14}H_{26}O$	210.35
1-Hexacosanol	$C_{26}H_{54}O$	382.70
1,19-Eicosadiene	$C_{20}H_{38}$	278.51

Table 4. Qualitative phytochemicals screening of the ethanolic leaf extract of Meliceae family.

Bioactive component	Present in Meliceae family extract
Flavonoids	+++
Saponins	++
Tannins	+++
Alkaloids	++
Terpernoids	+
Phenolic Acid	+

Table 5. GC–MS analysis of bioactive compounds of extraction from Penaeus monodon shell

Compound name	Molecular formula	Molecular weight
Pyridine	C_5H_5N	79.10
Acetamide	C_2H_5NO	59.07
2-Pyridinecarboxaldehyde	C_6H_5NO	107.11
N-Acetyl-N-ethenylacetamide	$C_6H_9NO_2$	127.14
Acetylpyridone	C_7H_7NO2	137.14
3-Acetamidofuran	$C_7H_7NO_2$	125.13
3-Acetamido-5-methylfuran	$C_7H_9NO_2$	139.15
3-Acetamido-4-pyrone	$C_7H_7NO_3$	153.14
Oxazoline derivatives	C_3H_5NO	71.08
Dianhydro-2-acetamido-2-deoxyglucose	$C_8H_{11}NO_4$	185.18
6-Anhydro-2-acetamido-2-deoxyglucose	$C_8H_{13}NO_5$	203.19

Table 6. GC–MS analysis of bioactive compounds in ethanol leaf extract of Annonaceae family.

Compound name	Molecular formula	Molecular weight
Cyclandelate	$C_{17}H_{24}O_3$	276.3707
Phenol, 4-(methoxymethyl)-	$C_8H_{10}O_2$	138.1638
6, 6-Diphenylfulvene	$C_{18}H_{14}$	230.3038
Eicosane	$C_{20}H_{42}$	282.5475
di-a-Tocopherol	$C_{29}H_{50}O_2$	430.7061
Vitamin E	$C_{29}H_{50}O2$	430.7061
7-Oxabicycloheptane, 1-methyl-4-	$C_{10}H_{16}O_2$	168.2328
Cubenol	$C_{15}H_{18}O_2$	222.3663
Geranyl isovalerate	$C_{15}H_{26}O_2$	238.3657
Dodecane, 1,1,2-dibromo-	$C12H24Br2$	328.127

Table 7. Qualitative phytochemicals screening of the ethanolic extract of Annonaceae family.

Bioactive component	Present in Annonaceae family extract
Flavonoid	+++
Saponins	+
Tannins	+++
Alkaloids	++
Phenol	++
Glycoside	++

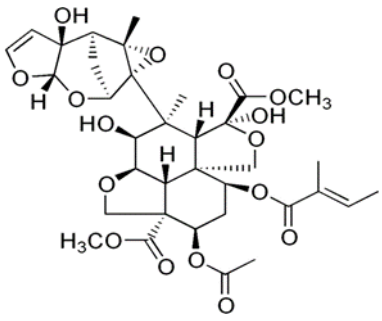

Figure 1. Chemical structure of Meliaceae family extract.

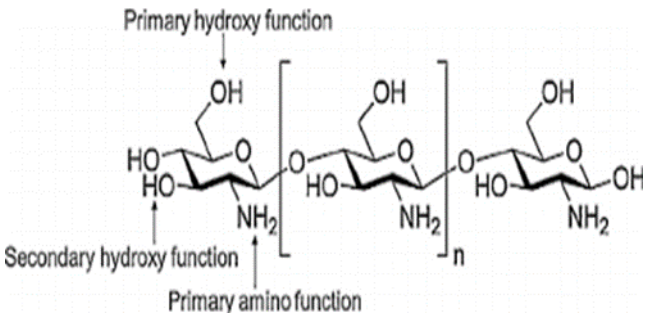

Figure 2. Chemical structure of Penaeus monodon extract (PE).

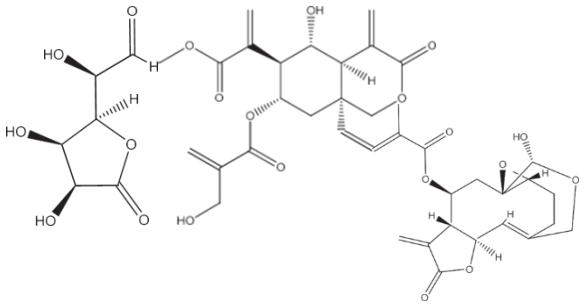

Figure 3. Chemical structure of Asteraceae family extract.

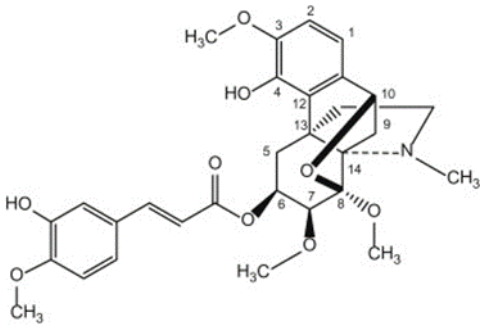

Figure 4. Chemical structure of Annonaceae family extract.

The experimental setup consisted of a closed mini-hydrate flow loop, as illustrated in Figure 5.

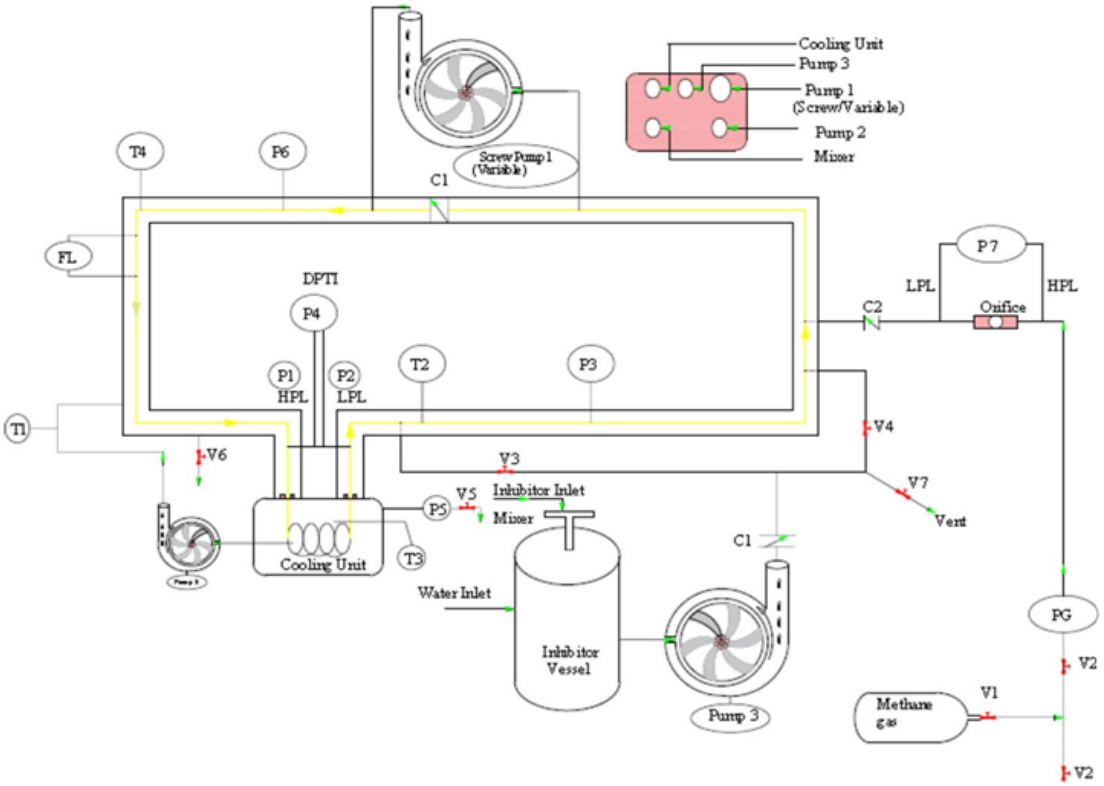

Figure 5. Schematic diagram of gas hydrate flow loop.

The flow loop has an overall diameter of 39.4 inches, constructed from 316 stainless steel tubing with an internal diameter of 0.5 inches, enclosed within a 4-inch polyvinylchloride (PVC) pipe. The entire system is mounted on an external metal frame. It includes six pressure gauges, three temperature gauges, a visual flow meter to monitor fluid flow, a compressed natural gas (CNG) cylinder, a mixing vessel for combining water and inhibitors in different weight percentages, three pumps, and a control panel to operate and power the loop.

The experiment was started by powering the main system and control panel. Next, pump 3 and valve 4 were activated to transfer water from the mixing vessel into the inner line until the pressure reached 25 psi. After this point, both pump 3 and valve 4 were turned off, and valve 7 was opened to flush out the water. This flushing process was repeated to ensure the system was free of rust and debris. For the hydrate formation experiment, once the pressure reached 25 psi, the CNG bottle was opened, and valve 1 along with the orifice was activated to raise the pressure to 150 psi. Once the desired pressure was achieved, both valve 1 and the orifice were closed. Pump 2 was switched on to circulate the cooling water through the

PVC pipe, and pump 1 was set at 150 psi to facilitate proper mixing of the gas and water. Ice cubes were added to rapidly cool the system, promoting hydrate formation. Temperature and pressure data were recorded every two minutes for a duration of two hours. During hydrate inhibition testing, different concentrations of inhibitors were introduced into the system, following the same procedure, with temperature and pressure monitored every two minutes over the entire two-hour period. The loop operated as a closed system, designed to allow temperature and pressure fluctuations based on phase changes. To minimise experimental errors, readings were taken three times under controlled conditions. The loop was flushed before each experiment to remove rust or debris, ensuring no gas remained trapped, and the gauges were checked to ensure proper functioning and to avoid interference [13,19,35-36].

3. Result and discussion

3.1. Suppression performance for uninhibited system

Graphs of pressure and temperature over time from hydrate formation experiments were analysed to assess inhibitor effectiveness using a mini flow loop at concentrations of 0.01 wt%, 0.02 wt%, and 0.03 wt%. Figure 6 presents results without an inhibitor: pressure decreased from 150 psi to 120 psi within 10 minutes, reaching 102 psi at 40 minutes, 80 psi after one hour, and stabilising at 36 psi after 100 minutes due to hydrate nucleation. Temperature initially fell from 30°C to 25°C but increased to 29.5°C by the end of the experiment, driven by methane diffusion and the exothermic heat release from hydrate crystallisation. This was attributed to the fact that hydrate formation is an exothermic process [37].

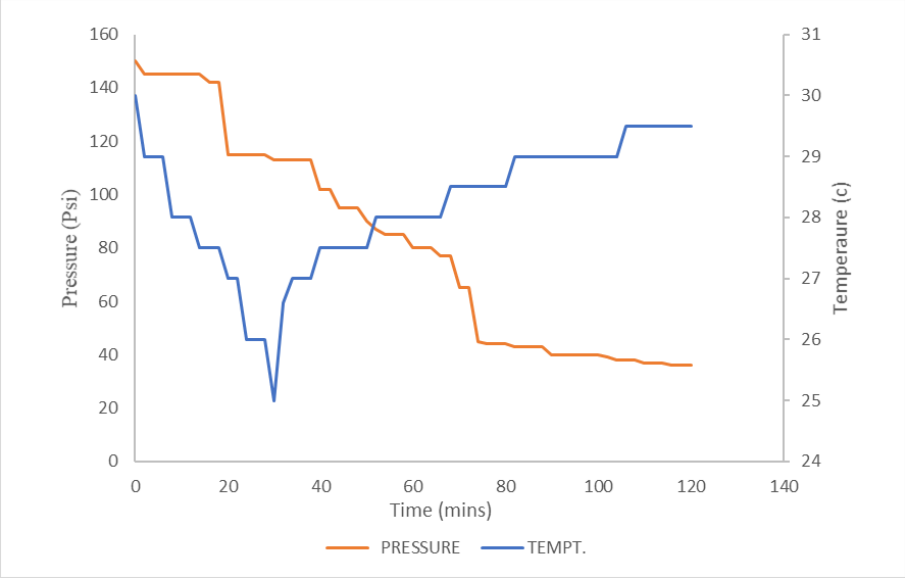

Figure 6. Pressure against temperature for uninhibited system.

3.2. Performance analysis of pressure for Asteraceae extract (AE), Meliaceae extract (ME), Annonaceae extract (ANE), Penaeus monodon extract (PE), 2-(Dimethylamino) ethylmethacrylate (2-DIMETH) and uninhibited pressure

The inhibitors' performance was assessed through pressure versus time plots at different weight percentages, showing the gradual pressure decreases and stabilisation over time as illustrated in Figures 7, 8, and 9. Each inhibitor demonstrated distinct behaviour under similar conditions.

AE demonstrated the most effective inhibition performance. At 0.01 wt%, the pressure initially dropped from 150 psi to 145 psi within the first 2 minutes. Over the next 15 minutes, the pressure gradually decreased further to 139 psi, where it stabilised for the following 30 minutes. Over the next 60 minutes, the pressure further dropped to 125 psi, and at 120

minutes, it was reduced to 120 psi. At 0.02 wt%, the pressure decreased from 150 psi to 144 psi in the first 2 minutes, reached 142 psi after 20 minutes, declined to 134 psi after 40 minutes, then reduced to 129 psi after 60 minutes. It further decreased to 126 psi after 90 minutes and was maintained at this level until the end of 120 minutes. Similarly, at 0.03 wt%, the pressure declined from 150 psi to 140 psi in 2 minutes, stabilised at 134 psi after 20 minutes, and remained stable until 60 minutes, after which it declined to 130 psi and was maintained until 120 minutes. Its consistent performance is linked to its hydroxyl-rich bioactive compounds, such as saponins, tannins, alkaloids, phenolic acids, and flavonoids, which effectively interfere with hydrate cage formation.

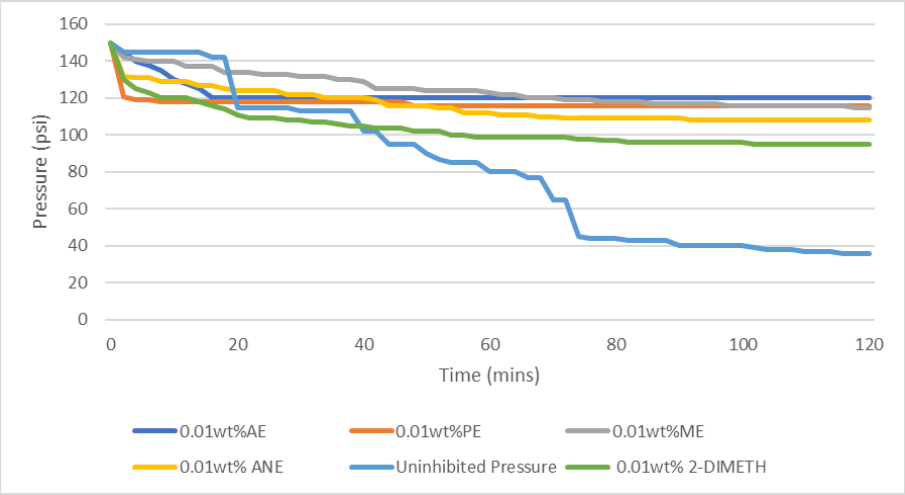

Figure 7. Pressure against time for 0.01wt% of AE, PE, ME, ANE, 2-DIMETH and uninhibited pressure.

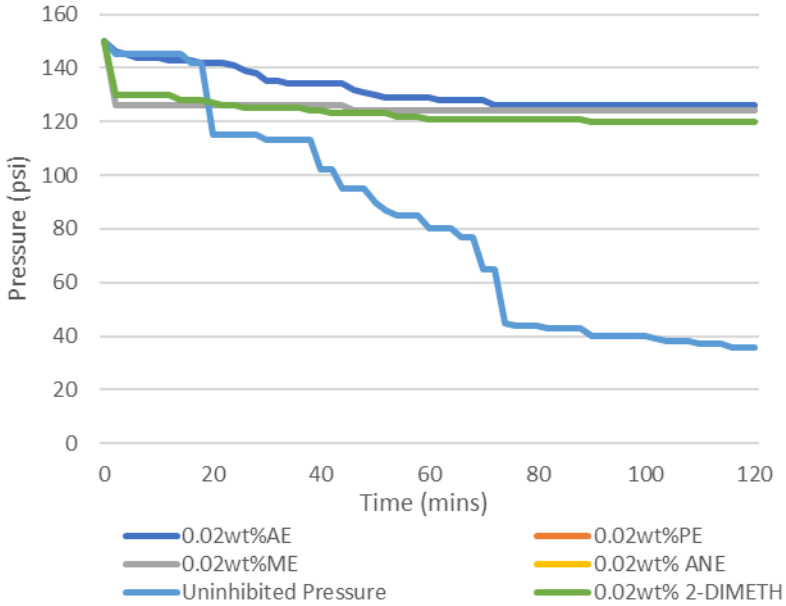

Figure 8. Pressure against time for 0.02wt% of AE, PE, ME, ANE, 2-DIMETH and uninhibited pressure.

For ME, at 0.01 wt.%, the pressure initially dropped from 150 psi to 142 psi within the first 2 minutes. Over the next 20 minutes, the pressure further decreased to 134 psi, where it stabilised for the following 30 minutes. Over the subsequent 60 minutes, the pressure gradually declined to 127 psi and further dropped to 115 psi by the end of 120 minutes. At 0.02 wt.%, the pressure dropped from 150 psi to 144 psi in the first 2 minutes, reached 138 psi after 20 minutes, and continued to decline to 132 psi after 40 minutes. The pressure then

reduced to 128 psi after 60 minutes, before falling further to 109 psi at the end of 120 minutes. At 0.03 wt%, the pressure initially decreased from 150 psi to 126 psi within 2 minutes, stabilising at 137 psi after 20 minutes, and maintained this level for the next 40 minutes. After 60 minutes, the pressure declined further to 132 psi, and at the end of 120 minutes, it stabilised at 129 psi. The performance of ME is attributed to its bioactive compounds, which are rich in peptides and polysaccharides, disrupting hydrate cage formation.

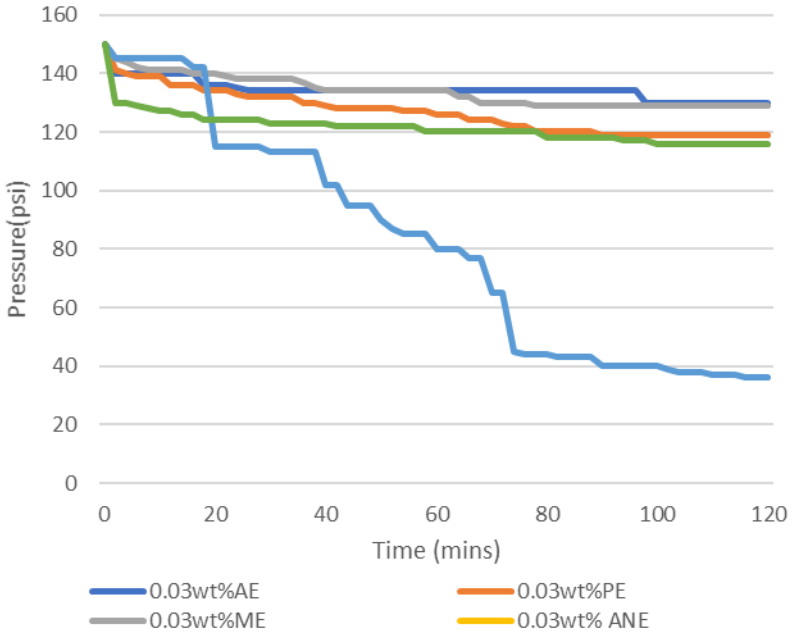

Figure 9. Pressure against time for 0.03wt% of AE, PE, ME, ANE, 2-DIMETH and uninhibited pressure.

At 0.01 wt.%, the pressure initially dropped from 150 psi to 145 psi within the first 2 minutes. Over the next 15 minutes, it further decreased to 139 psi, where it stabilised for 30 minutes. During the following 60 minutes, the pressure decreased to 126 psi, and by the end of 120 minutes, it reached 108 psi. At 0.02 wt.%, the pressure fell from 150 psi to 144 psi in the first 2 minutes, then declined to 138 psi after 20 minutes, and further decreased to 133 psi after 40 minutes. Over the following 60 minutes, pressure decreased to 127 psi and ultimately reached 123 psi at 120 minutes. At 0.03 wt.%, the pressure initially reduced from 150 psi to 142 psi within 2 minutes, stabilised at 135 psi after 20 minutes, and maintained this level for 60 minutes. Subsequently, the pressure fell to 130 psi and stabilised at 119 psi by the end of 120 minutes.

PE showed moderate effectiveness in inhibiting hydrate formation, with consistent pressure decreases over time. At 0.01 wt.%, the pressure fell from 150 psi to 147 psi within 2 minutes. Over the subsequent 15 minutes, it gradually decreased to 143 psi and then remained stable for 30 minutes. During the next 60 minutes, the pressure further dropped to 130 psi, reaching 116 psi at the 120-minute mark. At 0.02 wt.%, the pressure initially declined from 150 psi to 146 psi within 2 minutes, then to 140 psi after 20 minutes, and further to 135 psi after 40 minutes. Over the following 60 minutes, it reduced to 129 psi, and by the end of 120 minutes, it was at 124 psi. At 0.03 wt.%, the pressure decreased from 150 psi to 145 psi within 2 minutes, stabilising at 138 psi after 20 minutes and maintaining this level for 40 minutes. During the next 60 minutes, it decreased to 133 psi, and at 120 minutes, it stabilised at 118 psi.

For 2-DIMETH, at 0.01 wt%, the pressure initially dropped from 150 psi to 140 psi within 2 minutes, then decreased to 130 psi after 15 minutes, and stabilised at 125 psi for 30 minutes. Over the next 60 minutes, the pressure reduced to 110 psi, and by the end of 120 minutes, it reached 95 psi. At 0.02 wt%, the pressure decreased from 150 psi to 138 psi in 2 minutes, declined further to 128 psi after 15 minutes, and stabilised at 122 psi for the following 30 minutes. Over the next 60 minutes, the pressure dropped to 127 psi, and at the end of

120 minutes, it reached 120 psi. At 3 wt%, the pressure initially dropped from 150 psi to 137 psi within 2 minutes, decreased to 125 psi after 15 minutes, and stabilised at 120 psi for the subsequent 40 minutes. Over the next 60 minutes, the pressure reduced to 115 psi, and by the end of 120 minutes, it stabilised at 116 psi.

AE consistently exhibited superior inhibition performance across all concentrations, effectively reducing pressure drops and delaying hydrate crystallisation. This outstanding performance is attributed to AE's high hydroxyl group content and abundant bioactive compounds, such as saponins, tannins, alkaloids, phenolic acids, and flavonoids, which disrupt water molecules' ability to form hydrate cages.

3.3. Performance analysis of temperature for Asteraceae extract (AE), Meliaceae extract (ME), Annonaceae extract (ANE), Penaeus monodon extract (PE), and 2-(Dimethylamino)ethylmethacrylate (2-DIMETH)

The temperature performance of the inhibitors AE, ME, ANE, PE, 2-DIMETH, and Uninhibited Temperature was assessed by analysing the temperature versus time profiles at various weight percentages (0.01 wt.%, 0.02 wt.%, and 0.03 wt.%) in Figures 10, 11, and 12. The controlled decline in temperature emphasises the inhibitory effects of these compounds on hydrate formation.

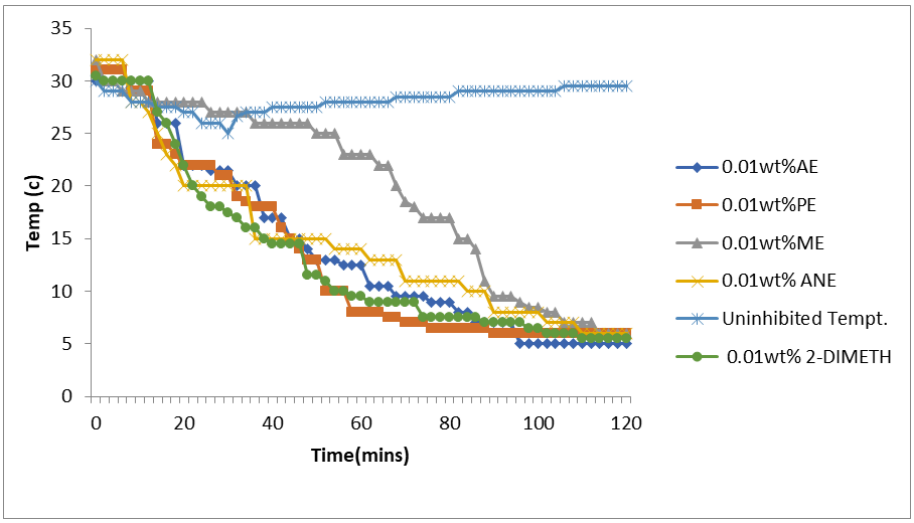

Figure 10. Temperature against time for 0.01wt% of AE, PE, ME, ANE, 2-DIMETH and uninhibited pressure.

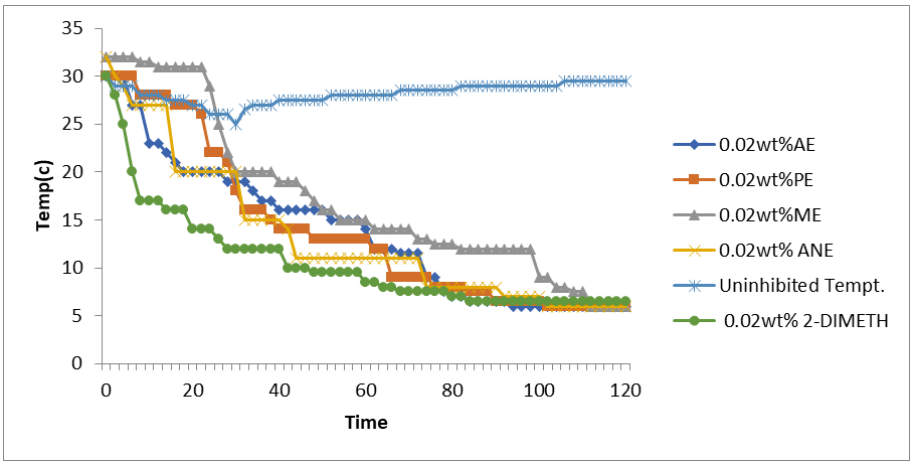

Figure 11. Temperature against time for 0.02 wt% of AE, PE, ME, ANE, 2-(Dimethylamino)ethylmethacrylate and uninhibited pressure.

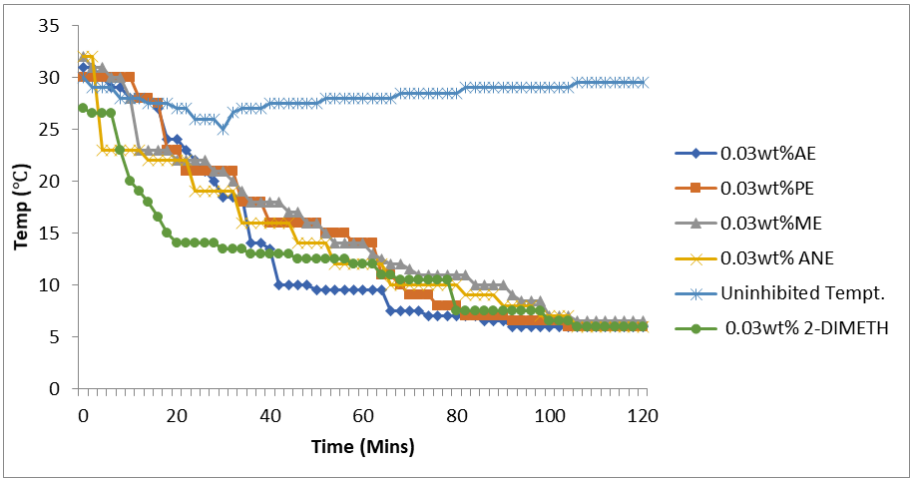

Figure 12. Temperature against time for 0.03 wt% of AE, PE, ME, ANE, 2-DIMETH and uninhibited pressure.

For AE, at 0.01 wt.% the temperature decreased from 32°C to 5.0°C, showing a steady decline and effective inhibition of hydrate formation. For ME, the temperature dropped from 30°C to 6.5°C, demonstrating its capacity to regulate temperature variation in the system. For ANE, the temperature reduced from 31°C to 6°C, indicating moderate effectiveness in delaying hydrate crystallization. For PE, the temperature declined from 29°C to 6°C, reflecting its ability to stabilize the system against hydrate growth. For 2-DIMETH, the temperature decreased from 30.5°C to 6.5°C, indicating slightly less effective performance in temperature regulation compared to the other inhibitors. At 0.02wt% For AE, the temperature reduced from 28°C to 6.0°C, indicating consistent performance in hydrate inhibition. For ME, the temperature dropped from 30°C to 6.5°C, showing a steady decline and effective stabilization of the system. For ANE, the temperature decreased from 29°C to 6°C, reflecting its ability to regulate temperature variation effectively. For PE, the temperature reduced from 28°C to 6°C, showcasing moderate inhibition performance. For 2-DIMETH, the temperature dropped from 30°C to 6.5°C, with its inhibitory action slightly less pronounced compared to AE and ME. At 0.03 wt.% for AE, the temperature dropped from 32°C to 6°C, demonstrating superior inhibition performance across all concentrations. For ME, the temperature reduced from 30°C to 6°C, maintaining consistent performance in hydrate regulation. For ANE, the temperature declined from 28°C to 6°C, reflecting moderate effectiveness in delaying hydrate nucleation. For PE, the temperature decreased from 29°C to 6°C, exhibiting a controlled decline in temperature. For 2-DIMETH, the temperature reduced from 27°C to 6°C. The consistent and steady decline in temperature for all inhibitors reflects their ability to delay hydrate formation by controlling the exothermic crystallization process and regulating system temperature.

3.4. Initial (P_i) and final pressure (P_f) pressure plots for AE, PE, ME, ANE, 2-DIMETH and uninhibited experiment

The initial and final pressures, along with pressure changes, were measured for the uninhibited system and for 0.01 to 0.03 wt.% of AE, ME, ANE, PE, and 2-DIMETH, as shown in Figures 13, 14, and 15. The initial pressures for all experiments were standardised to 150 psi. However, the final pressures varied since gas was consumed during the experiments. Consequently, differences between the final pressures for the uninhibited system and each inhibitor system illustrate how effectively these inhibitors prevented hydrate formation. A higher final pressure indicates a better inhibitor, as it reflects less gas consumption during hydrate formation. Conversely, a lower final pressure suggests less effective inhibition. For the uninhibited system, the loop is more prone to hydrate formation. The final pressure for this system was 51 psi, with a pressure change of 99 psi. Among all natural inhibitors, AE achieved the highest final pressure and the lowest change in pressure.

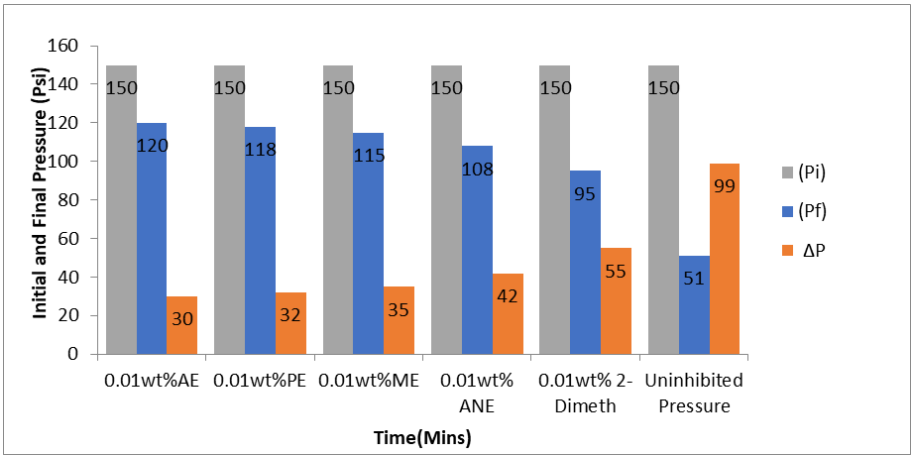

Figure13. Pressure versus time for 0.01 wt% of AE, PE, ME, ANE, 2-(dimethylamino)ethylmethacrylate and uninhibited experiments.

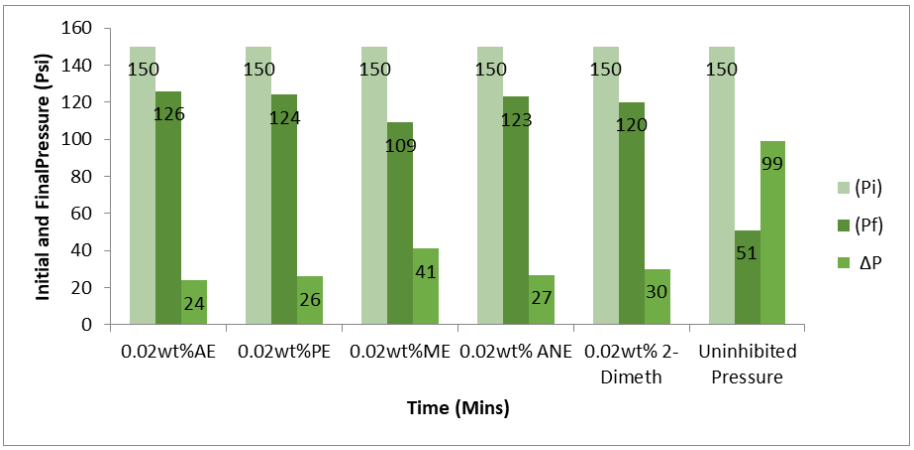

Figure 14. Pressure versus time for 0.02 wt% of AE, PE, ME, ANE, 2-DIMETH and uninhibited experiment.

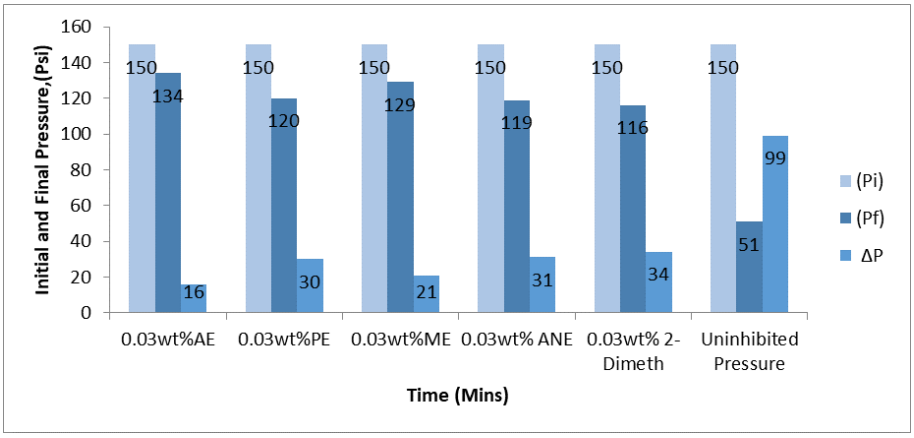

Figure 15. Pressure versus time for 0.03 wt% of AE, PE, ME, ANE, 2-DIMETH and uninhibited experiment.

The highest final pressures recorded were 120 psi, 126 psi, and 134 psi for concentrations of 0.01, 0.02, and 0.03 wt.%, respectively. The corresponding pressure changes at these concentrations were 30 psi, 24 psi, and 16 psi. For 2-DIMETH, at 0.01 to 0.03 wt.%, the final pressures measured were 95 psi, 120 psi, and 116 psi, with pressure changes of 55 psi, 30 psi, and 34 psi, respectively. From this analysis, AE demonstrated the most consistent perfor-

mance, showing higher final pressures and lower pressure changes across all weight percentages. However, 2-DIMETH exhibited the lowest pressure at 0.01 wt.%, with a final pressure of 95 psi and the highest pressure change of 55 psi (see Figures 13 to 15).

3.5. Inhibition efficiency of inhibitors

The inhibition efficiency (IE) of the system at various weight percentages of the inhibitors was determined using the formula below to evaluate their capacity for inhibition [13,16].

$$IE = (1 - X)\% \quad (1)$$

$$X = \Delta P_{inhibited} / \Delta P_{uninhibited} \quad (2)$$

$$\Delta P_{inhibited} = (P_i - P_f)_{inhibited} \quad (3)$$

$$\Delta P_{uninhibited} = (P_i - P_f)_{uninhibited} \quad (4)$$

where; X is the change in pressure of inhibited system divided by cthe hange in uninhibited system; P_i refers to initial pressure of the system (inhibited or uninhibited); P_f is the final pressure of the system (inhibited or uninhibited); $\Delta P_{inhibited}$ is the initial pressure minus final pressure of inhibited system; $\Delta P_{uninhibited}$ is the initial pressure minus final pressure of uninhibited system.

The Figure 16 compares the inhibition efficiency (IE) of various inhibitors at 0.01 wt.%, 0.02 wt.% and 0.03 wt.% concentrations. AE showed the highest efficiency, with IE values of 69.7%, 75.7%, and 83.8% respectively. ME had the inhibition efficiency of 65.5%, 73.7%, and 67.6%, while ANE recorded 64.6%, 58.6%, and 78.8%. PE displayed moderate IE values of 57.6%, 72.7%, and 58.9%. Lastly, 2-(dimethylamino)ethylmethacrylate had the inhibition efficiency of 51.8%, 73.7%, and 68.9%. This analysis indicates that the AE is the most efficient of all these inhibitors.

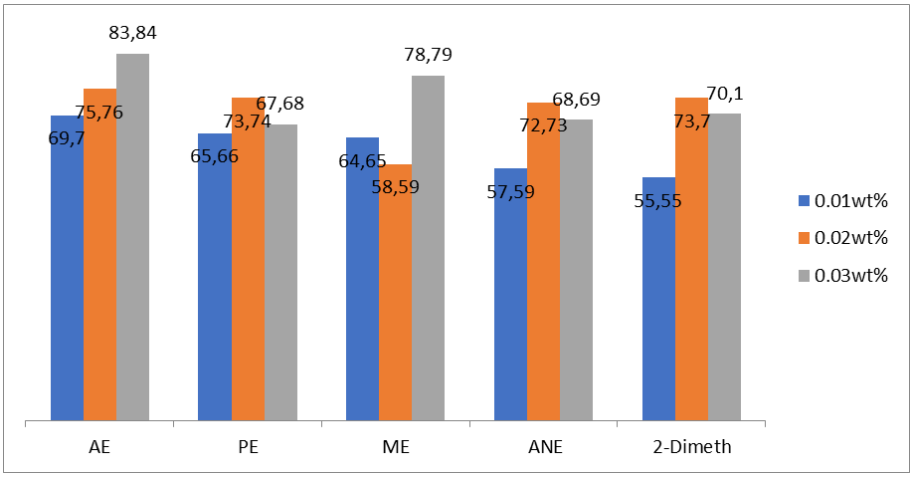

Figure 16. Inhibition efficiency versus weight for 0.01 wt%, 0.02 wt%, 0.03 wt% of AE, PE, ME, ANE and 2-DIMETH.

4. Conclusion

According to the experimental results, AE exhibited the highest inhibition efficiency among the inhibitors under test; this is reflected through the various pressure and temperature versus time plots. However, ME, ANE, and PE showed fairly good inhibition performance, but on the other side, AE maintained better performance among all weight percentages. The kinetic inhibitor 2-(Dimethylamino) ethylmethacrylate performed moderately but not quite better than AE. Given its effectiveness, eco-friendliness and biodegradability, AE is recommended for further field trials as a sustainable alternative to conventional gas hydrate inhibitors.

Acknowledgement

The authors acknowledge the Institute of Petroleum and Energy Studies and the Department of Petroleum and Gas Engineering, University of Port Harcourt, Nigeria for their support in carrying out this research in their laboratories.

Authors' contribution

All authors contributed to the study, conception and design. Nakwaasah Otua Ledum and Okon Efiong Okon contributed to material preparation and data collection. Nakwaasah Otua Ledum analyzed data and prepared the first draft. Okon Efiong Okon contributed to editing and reviewing of draft manuscript. Uche Osokogwu also reviewed manuscript. Uche Osokogwu contributed to supervision and comments on previous version of manuscripts.

Conflict of interest

The authors whose names are listed above certify that they have no affiliation or involvement in any organization or entity with any financial interest or non-financial interest in the subject matter or material discussed in this manuscript.

References

[1] Sloan ED. Clathrate Hydrates of Natural Gases. 2nd Edition 2003, Marcel Dekker Inc., New York.

[2] Makogon YF. Hydrates of Hydrocarbons. PennWell Publishing Company. 1997

[3] Kvenvolden KA. Gas hydrates—geological perspective and global change, Reviews of Geophysics 1993, https://doi.org/10.1029/93RG00268

[4] Koh CA, Sum AK, and Sloan ED. State-of-the-art review of gas hydrates and their impact on flow assurance. Journal of Natural Gas Chemistry, 2002;11(3): 1-12.

[5] Sloan ED, and Koh CA. Clathrate Hydrates of Natural Gases. 3rd Edition 2007, CRC Press, Boca Raton.

[6] Gudmundsson JS, Borrehaug A. Frozen hydrate for transport of natural gas. In Proceedings of the 2nd International Conference on Natural Gas Hydrates 1996; (pp. 415–422).

[7] Hammerschmidt EG. Formation of Gas Hydrates in Natural Gas Transmission Lines. Industrial and Engineering Chemistry, 1934;26(8): 851–855.

[8] Sloan ED. A Changing Hydrate Paradigm-from apprehension to avoidance to risk management. Fluid Phase Equilibria, 2005; 228-229: 64–67.

[9] Bandyopadhyay S, Hoffmann R, and Kelland MA. Studies on the inhibition of hydrate growth with a kinetic inhibitor. Energy & Fuels, 2004;18(4): 1098–1104.

[10] Firoozabad A. Gas hydrates: A review of hydrate inhibitors. Energy & Fuels, 2007; 21(2): 717-725.

[11] Kelland MA. History of the development of low dosage hydrate inhibitors. Energy & Fuels, 2006; 20(3): 825–847.

[12] Okon OE, Ajienka JA, Ikiensikimama SS, Elechi VU, Odutola TO. Use of Locally Formulated Inhibitor from Agro-Waste for Gas Hydrate Inhibition in a Mini Flow Loop. International Journal of Science and Engineering Investigations, 2018; 7(83): I04–112.

[13] Okon OE, Ikiensikimama SS, Wachikwu-Elechi VU, Ajienka JA and Akaranta OE. Gas hydrate inhibition: performance of an agro-waste based locally formulated inhibitor. Journal of Dispersion Science and Technology. 2022; 44(12): 2330-2339. https://doi.org/10.1080/01932691.2022.2074858

[14] Okon OE, Ajienka JA, Ikiensikimama SS, Akaranta, OE, and Wachikwu-Elechi VU. Experimental investigation and comparative environmental impact analysis of conventional and naturally occurring kinetic hydrate inhibitors in offshore environments using toxicity and bioconcentration tools, Results in Engineering, 2023; 21(1-12) https://doi.org/10.1016/j.rineng.2023.101705

[15] Okon OE, Ajienka JA, Ikiensikimama SS, and Akaranta OE. hytochemical characterization of selected agro-waste extracts as kinetic inhibitors in methane hydrates formation, Results in Engineering, 2024; 23(1-16) https://doi.org/10.1016/j.rineng.2024.102429

[16] Elechi VU, Ikiensikimama SS, Ajienka JA, Akaranta O, Onyekonwu MO, and Okon OE. (2019a). Comparative Analysis of Gas Hydrate Inhibitors: Local and Conventional. *SPE-197429,* presented at the Abu Dhabi International Petroleum Exhibition & Conference, Abu Dhabi, UAE, 11-14 November. https://doi.org/10.2118/197429-MS

[17] Elechi VU, Ikiensikimama SS, Ajienka JA, Akaranta OE, Onyekonwu MO, and Okon OE. Evaluation of the Inhibition Efficiency of Plant Extract PE as Gas Hydrate Inhibitor in a Simulated Offshore Environment. SPE-198781-MS. Society of Petroleum Engineers. Presented at the Nigeria Annual International Conference and Exhibition, Lagos, Nigeria, 5–7 August 2019. https://doi.org/10.2118/198781-MS

[18] Elechi VU, Ikiensikimama SS, Akaranta OE, Ajienka JA, and Okon OE. Investigation of Plant Family Costaceae Ex tract as Gas Hydrate Inhibitor in a Simulated Offshore Environment. International Journal of Science and Engineering Investigations, 8(84), January 2019.
[19] Elechi VU, Ikiensikimama SS, Akaranta OE, Ajienka JA, Onyekonwu MO, and Okon OE. The use of a bench-scale high-pressure apparatus to evaluate the effectiveness of a locally sourced material as gas hydrate inhibitor. Journal of Natural Gas Science and Engineering, 2020; 74: 103022. https://doi.org/10.1016/j.jngse.2020.103022
[20] Odatuwa T, Osokogwu U, and Okon OE. (2022). Experimental investigation of plant family extracts as gas hydrate inhibitors in an offshore simulated environment. Petroleum Science and Technology. 2022; 42(11): 1413-1430. https://doi.org/10.1080/10916466.2022.2144358
[21] Cheng L, Cui J, Li J, Zhu R, Liu B, Ban S, and Chen G. High efficient development of green kinetic hydrate inhibitors via combined molecular dynamic simulation and experimental test approach. Green Chemical Engineering, 2022; 3(1): 34-43 https://doi.org/10.1016/j.gce.2021.07.010.
[22] Mbooh TR, Osokogwu U, Okon O E, Akwa-Abasi US. Evaluation of Hybrid Hydrate Inhibitor in Dissociating Hydrate Formation in Offshore Flowlines. Petroleum and Coal, 2021; 63(3): 636-645.
[23] Madueke SC, Osokogwu U, and Okon OE. Evaluating the Performance of Deep Eutectic Solvent using Synergetic Compounds in Gas Hydrate Inhibition, Petroleum and Coal, 65(2): 353-362.
[24] Kakwaya JP, Madirisha MM, Kilulya KF, Lugwisha EHJ. Isolation and Performance Test of Green Low Dosage Hydrate Inhibitors from Local Materials for Improving Flow Assurance in Oil and Gas Industry, Tanzania Journal of Engineering and Technology, 2023; 42(2)*: 95-112. https://doi.org/10.52339/tjet.v42i2.806
[25] Potts M, Sutton K, and Pereira L. Bioactive compounds in Annonaceae plants: Uses in medicine and biotechnology. Journal of Plant Research, 2012; 125(4): 349–357.
[26] Matsushige K, Kotake Y, and Mori, M. Bioactive alkaloids from Annonaceae plants. Journal of Natural Products, 2012; 75(10): 1825–1832.
[27] Harborne JB, Williams CA. Advances in flavonoid research since 1992. Phytochemistry, 2000;55(6), 481-504. https://doi.org/10.1016/S0031-9422(00)00235-1
[28] Kumar S, and Pandey AK. Chemistry of Biological Activities of Flavonoids: An Overview, The Scientific World Journal, 2013; 162750, https://doi.org/10.1155/2013/162750
[29] Stephen H, and Peter T. Solubilities of Inorganic and Organic Compounds: A Critical Review of Data. Pergamon Press 2000.
[30] Stephen A, and Peter T. Phytochemical properties of Asteraceae: Medicinal and nutritional uses. Journal of Ethnopharmacology, 2000; 73(3): 323–332.
[31] Haslam E. Practical polyphenolics: From structure to molecular recognition and physiological action. Cambridge University Press 1998.
[32] Francis G, Kerem Z, Makkar HP, and Becker K. The biological action of saponins in animal systems: A review. British Journal of Nutrition, 2002; 88(6): 587-605. https://doi.org/10.1079/BJN2002725
[33] Sparg SG, Light ME, and van Staden J. Biological activities and distribution of plant saponins. Journal of Ethnopharmacology, 2004; 94(2-3): 219-243. https://doi.org/10.1016/j.jep.2004.05.016
[34] Quideau S. Chitosan as a biopolymer in natural gas hydrate inhibition. Bioorganic & Medicinal Chemistry, 2011; 19(22): 6704–6711.
[35] Odutola TO, Ajienka JA, Onyekonwu MO, and Ikiensikimama SS. Design, Fabrication and Validation of a Laboratory Flow Loop for Hydrate Studies. American Journal of Chemical Engineering, 2017; 5(3): 28-41.
[36] Ripmeester JA, Tse JS, Ratcliffe CI, and Powell BM. Gas hydrates: From laboratory curiosities to potential and challenges of industrial applications. Chemical Reviews, 2005; 105(3): 920–938. https://doi.org/10.1021/cr000376p
[37] Movareji MK, Charffarknah A, and Sadeghi A. Effect of three representative surfactant on methane hydrate formation rate and induction time. Egyptian Journal of Petroleum, 2016; 26: 231–339.

To whom correspondence should be addressed: Okon Efiong Okon, World Bank Africa Centre of Excellence in Oilfield Chemicals Research (ACE-CEFOR), University of Port Harcourt, Choba, Rivers State, Nigeria
E-mail: okon_okon@uniport.edu.ng